Hindawi
Journal of Nanomaterials
Volume 2022, Article ID 4761989, 9 pages
https://doi.org/10.1155/2022/4761989

Research Article

Cooling a Hot Semiannulus with Constant Heat Flux by Using Fe_3O_4-Water Nanofluid and a Magnetic Field: Natural Convection Mechanism

Zhengqiang Yang,[1] S. M. Bouzgarrou,[2,3] Riadh Marzouki,[4] Fatma Aouaini,[5] M. A. El-Shorbagy,[6,7] Mahidzal Dahari,[8] Said Anwar Shah,[9] and D. L. Suthar[10]

[1]*School of Computer Science and Engineering, Xi'an Technological University, Xi'an 710021, China*
[2]*Civil Engineering Department, Faculty of Engineering, Jazan University, Saudi Arabia*
[3]*Higher Institute of Applied Sciences and Technologie of Sousse, Sousse University, Tunisia*
[4]*Department of Chemistry, College of Science, King Khalid University, Abha 61421, Saudi Arabia*
[5]*Department of Physics, College of Science, Princess Nourah bint Abdulrahman University, P.O. Box 84428, Riyadh 11671, Saudi Arabia*
[6]*Department of Mathematics, College of Science and Humanities in Al-Kharj, Prince Sattam Bin Abdulaziz University, Al-Kharj 11942, Saudi Arabia*
[7]*Department of Basic Engineering Science, Faculty of Engineering, Menoufia University, Shebin El-Kom 32511, Egypt*
[8]*Department of Electrical Engineering, Faculty of Engineering, University of Malaya, 50603 Kuala Lumpur, Malaysia*
[9]*Department of Basic Science and Islamiyat, University of Engineering and Technology, Peshawar, Pakistan*
[10]*Department of Mathematics, Wollo University, P.O. Box 1145, Dessie, Ethiopia*

Correspondence should be addressed to D. L. Suthar; dlsuthar@gmail.com

Received 13 January 2022; Revised 8 February 2022; Accepted 5 April 2022; Published 26 May 2022

Academic Editor: Taza Gul

In this simulation, the nanoparticle distribution and entropy generation were studied using the Buongiorno's developed two-phase model and magnetic field inside a porous semiannulus cavity. The influence of three terms was considered in the Buongiorno's developed two-phase model such as Brownian motion, thermophoresis, and magnetophoresis effects. In addition, the entropy generation was assessed due to temperature and velocity gradient. The evidence showed that the effects of the magnetic field in high porosities and volume fraction of nanoparticles were remarkable on the Nusselt number and entropy generation. Also, irreversibility due to heat transfer is much greater than fluid friction.

1. Introduction

Nowadays, heat transfer processes have widely exerted for many applications such as cooling battery, CPU, forging, radiator in vehicles, heating the home, and powerplant [1–5]. One method that is popular between thermal engineering is injecting various nanoparticles such as metal, nonmetal, and oxide nanoparticles and nanoencapsulated phase change material (NEPCM) to host fluid [6–8], because mixing nanoparticles into host fluid can changed the thermophysical properties, specifically, thermal conductivity of host fluid [9–11].

In recent years, the heat transfer rates by computational fluid dynamics (CFD) and entropy generation are significantly investigated by researchers and companies due to having accurate with experimental studies [12–15]. Moreover, owing to its large specific area and higher solid thermal conductivity, there has been growing interest in heat transfer inside the porous media. According to previous studies, porous structure improves thermal performance of nanofluid [16–19]. A numerical investigation of heat transfer and fluid flow in a parabolic trough solar receiver with internal annular porous structure and synthetic oil-Al_2O_3 nanofluid was carried out by Bozorg et al. [20]. According to their results, utilization of porous structure and nanofluids enhances heat transfer coefficient 7% and 20%, respectively. Jamal-Abad et al. [21] experimentally studied the thermal efficiency of a solar parabolic trough collector filled with porous media; they illustrated an enhancement in efficiency of the collector by increasing the mass flow rate.

It is confirmed that in nanofluid simulation, two-phase approach provides better accuracy compared to single-phase approach [22–24]. A two-phase model presented by Buongiorno [25] has received significant attention; in this model, it is suggested that among seven slip mechanisms, Brownian motion and thermophoresis diffusion play vital role in nanofluid distribution. Natural convection of nanofluid in an inclined cavity and inside porous medium considering two-phase approach is studied by studies [6] and [15]. Their results demonstrate good agreement with experimental studies. Thermophoresis and Brownian motion effect on boundary layer flow of nanofluid in presence of thermal stratification due to solar energy is analyzed by Anbuchezhian et al. [26]. Their results highlighted that Brownian motion and thermophoresis distribution can affect the heat transfer properties; they reported a substantial impact on the boundary layer flow field by Brownian motion in the presence of thermal stratification. Kaloudis et al. [27] numerically investigated on parabolic trough solar collector with nanofluid using a two-phase model. They reported that two-phase simulation of nanofluids in solar studies shows better agreement with experimental studies. Also, the presence of nanoparticles improves collector's efficiency.

To obtain the optimal configuration of solar collectors, it is essential to analyze the entropy generation. Farshad and Sheikholeslami [28] scrutinize exergy loss and heat transfer of mixture of aluminum oxide and H_2O through a solar collector. Thermal performance and entropy generation analysis of a high concentration ratio parabolic trough solar collector was studied by Mwesigye et al. [29]. They reported a decrement in entropy generation with augmentation of nanofluid volume fraction for some ranges of Re number. Verma et al. [30] experimentally analyzed exergy efficiency and entropy generation in flat plate solar collectors for different types of nanofluids. They highlighted that rise of Bejan number towards unity illustrates the improvement of system performance due to efficient conversion of the available energy into useful functions. Also, Sheikholeslami et al. [31] scrutinized impact of Lorentz forces on magnetic nano fluid of Fe_3O_4 with entropy and exergy analyzing inside a semiannulus. Afrand et al. [32] studied free convective heat transfer and entropy generation of Al_2O_3-water nanofluid in a triangular enclosure. They illustrated that the Bijan number increases by decreasing the Ra and increasing the Ha. The maximum heat transfer rate takes place at the enclosure angle of 60°.

To the best knowledge of the authors, there has been no detailed investigation of impacts of nonuniform magnetic fields on PTC thermal performance using nanofluid, considering Brownian motion and thermophoresis distribution as well as entropy generation. In the present work, a coil is wrapped around semiannulus to produce a variable magnetic field. Also, it focuses on the local distribution of nanoparticles, entropy generation due to fluid friction and heat transfer, and Nusselt number variation.

2. Physical Model

In the present study, 2-dimensional and steady-state natural convection is simulated in a semiannulus enclosure. Schematic presentation of the problem is presented in Figure 1. In Figure 1, two horizontal walls are thermally insulated, the inner semicircle wall at constant heat flux (q''), and the outer semicircle wall is fixed at constant temperature (T_c). The working fluid is Fe_3O_4-water nanofluid. Natural convection fluid flow is simulated based on Boussinesq's approximation. Also, heat transfer, nanoparticles distribution, and entropy generation in the presence of a nonuniform magnetic field are investigated. Therefore, it is assumed that nanoparticle distribution is based on Buongiorno two-phase model. According to the aforementioned assumption, the governing equations are presented in the next section.

3. Relations and Hypothesis

The nondimensional parameters are as follows: $X = x/L$, $Y = y/L$, $T^* = k_f(T - T_c)/\boldsymbol{q}''L$, $\boldsymbol{V}^* = \boldsymbol{V}L/\nu_f$, $P^* = PL^2/\rho_f \nu_f^2$, $\boldsymbol{H}^* = \boldsymbol{H}/H_0$, $\boldsymbol{M}^* = \boldsymbol{M}/M_0$, $\varphi^* = \varphi/\varphi_{\mathrm{Ave}}$,

$u^* = u/\alpha_f L$, $v^* = v/\alpha_f L$, $\nabla^* = L\nabla$, $\delta = k_f T_c/\boldsymbol{q}''L$, $D_B^* = D_B/D_{B0}$, $D_T^* = D_T/D_{T0}$, $D_{T0} = \gamma\mu_f/\rho_f\varphi_{\mathrm{Ave}}$,

$H_0 = I/2\pi\lambda$, $D_{B0} = K_B T_c/3\pi\mu_f d_{np}$, and $M_0 = \chi(\varphi_{\mathrm{Ave}}, T_f)H_0$ for $\varphi_{\mathrm{Ave}} = 0.02$, and $T_m = T_c + q''L/2k_f$.

The dimensionless forms of continuity equations, momentum, energy, and volume fraction are as follows:

Nondimensional continuity equation:

$$\nabla^*.\boldsymbol{V}^* = 0. \tag{1}$$

Nondimensional momentum equation:

$$\left(\frac{1}{\varepsilon^2}\frac{\rho_{nf}}{\rho_f}\right)(\boldsymbol{V}^*.\nabla^*)\boldsymbol{V}^* = -\nabla^* P^* - \left(\frac{\mu_{nf}}{\mu_f}\right)\frac{1}{Da}\boldsymbol{V}^* + \nabla^*.\left(\frac{\mu_{nf}}{\mu_f}\nabla^*\boldsymbol{V}^*\right)$$

$$+ \left(\frac{(\rho\beta)_{nf}}{\rho_f\beta_f}\right)\frac{Ra_f}{\mathrm{Pr}}T^*.\hat{\boldsymbol{e}} + Mn\,(\boldsymbol{M}^*.\nabla^*)\boldsymbol{H}^*. \tag{2}$$

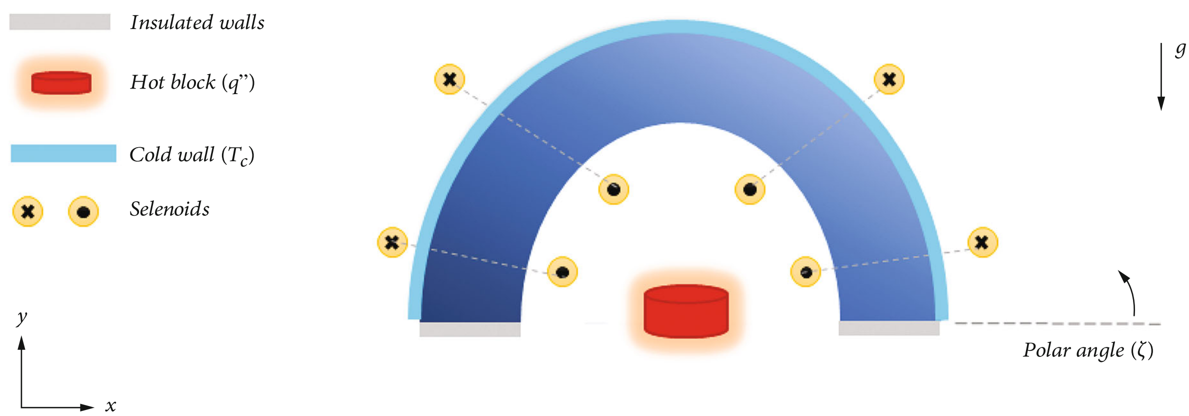

FIGURE 1: Schematic presentation of the problem.

Nondimensional heat transfer equation:

$$\frac{(\rho C_P)_{nf}}{(\rho C_P)_f} \boldsymbol{V}^*.\nabla^* T^* = \frac{1}{\Pr}\nabla^*\left(\frac{k_{eq}}{k_f}\nabla^* T^*\right) + \varepsilon\frac{1}{\Pr}\frac{1}{Le}\left(D_B^*\nabla^*\varphi^*.\nabla^* T^* + \frac{D_T^*}{N_{BT}}\frac{\nabla^* T^*.\nabla^* T^*}{1+(T^*/\delta)} - D_B^*\xi \boldsymbol{L}(\xi)\varphi^*\frac{\nabla^*\boldsymbol{H}^*.\nabla^* T^*}{\boldsymbol{H}^*}\right). \tag{3}$$

Nondimensional mass transfer equation:

$$\frac{1}{\varepsilon}\boldsymbol{V}^*.\nabla^*\varphi^* = \frac{1}{Sc}\nabla^* .\left(D_B^*\nabla^*\varphi^* + \frac{D_T^*}{N_{BT}}\frac{\nabla^* T^*}{1+(T^*/\delta)} - D_B^*\xi\boldsymbol{L}(\xi)\varphi^*\frac{\nabla^*\boldsymbol{H}^*}{\boldsymbol{H}^*}\right). \tag{4}$$

The dimensionless numbers in the above relationships are defined as:

$$Da = \frac{K}{L^2}, \Pr = \frac{\nu_f}{\alpha_f}, \alpha_f = \frac{k_f}{(\rho c_p)_f}, Ra_f = \frac{gB_f q'' L^4}{k_f\alpha_f\nu_f}, Ra_p = Ra_f Da, \hat{\boldsymbol{e}} = \frac{\boldsymbol{g}}{g}, Mn = \frac{\mu_0 H_0 M_0 L^2}{\rho_f\nu_f^2}, Le = \frac{k_f}{(\rho C_p)_{np} D_{B0}\varphi_{Ave}}, N_{BT} = \frac{\varphi_{Ave} D_{B0}\delta}{D_{T0}}, Sc = \frac{\nu_f}{D_{B0}}. \tag{5}$$

Mn is the magnetic number, which is defined as the ratio of the Kelvin force to the kinematic viscosity. Moreover, Da, Ra, Pr, Le, and Sc denote the Darcy, Rayleigh, Prandtl, Lewis, and Schmitt numbers, respectively.

The average Nusselt on the constant heat flux wall (inner cylinder wall) is calculated as follows:

$$Nu_{loc} = \frac{k_{eq}}{k_{eff}}\frac{1}{T^*}, Nu_{ave} = \frac{1}{\pi}\int_0^\pi Nu_{loc}(\zeta)d\zeta. \tag{6}$$

In this study, the entropy generation is considered due to the irreversibility of the velocity gradients and temperature gradients. According to Shavik et al. [33], the entropy generation is obtained as

TABLE 1: Comparison of total entropy generation ($S_{g,tot}$) and Bejan number (Be_{ave}), for $\Pr = 0.71$ and irreversibility ($X = 10^{-4}$).

	$Ra = 10^3$		$Ra = 10^5$	
	$S_{g,tot}$	Be_{ave}	$S_{g,tot}$	Be_{ave}
Present work	1.154	0.97	23.2	0.193
Shavik et al. [33]	1.15	0.97	23.27	0.194

$$s_s = \frac{\mu_{nf}}{T_m}\left[2\left(\frac{\partial u}{\partial x}\right)^2 + 2\left(\frac{\partial v}{\partial y}\right)^2 + \left(\frac{\partial u}{\partial y} + \frac{\partial v}{\partial x}\right)^2\right] + \frac{k_{nf}}{T_m{}^2}\left[\left(\frac{\partial T}{\partial x}\right)^2 + \left(\frac{\partial T}{\partial y}\right)^2\right]. \tag{7}$$

In the mentioned equation, the first and second terms are local entropy generation due to the fluid friction ($S_{L,FF}$) and the heat transfer ($S_{L,HT}$) irreversibility, respectively. Also, the dimensionless equation of entropy generation is as follows:

$$S_{L,HT} = \frac{k_{nf}}{k_f}\left(\frac{\partial T^*}{\partial X}\right)^2 + \left(\frac{\partial T^*}{\partial Y}\right)^2,$$

$$S_{L,FF} = X\frac{\mu_{nf}}{\mu_f}\left[2\left[\left(\frac{\partial u^*}{\partial X}\right)^2 + \left(\frac{\partial v^*}{\partial Y}\right)^2\right] + \left(\frac{\partial u^*}{\partial Y} + \frac{\partial v^*}{\partial X}\right)^2\right], X = \mu_f k_f T_m\left(\frac{\alpha_f}{L^2 q''}\right)^2,$$

$$S_{L,s} = s_s \times \frac{k_f T_m{}^2}{q''^2} = S_{L,FF} + S_{L,HT}. \tag{8}$$

Bejan number is the ratio of the entropy generation due to the heat transfer to the total entropy generation. This is as follows:

$$Be_L = \frac{S_{L,HT}}{S_{L,s}}. \tag{9}$$

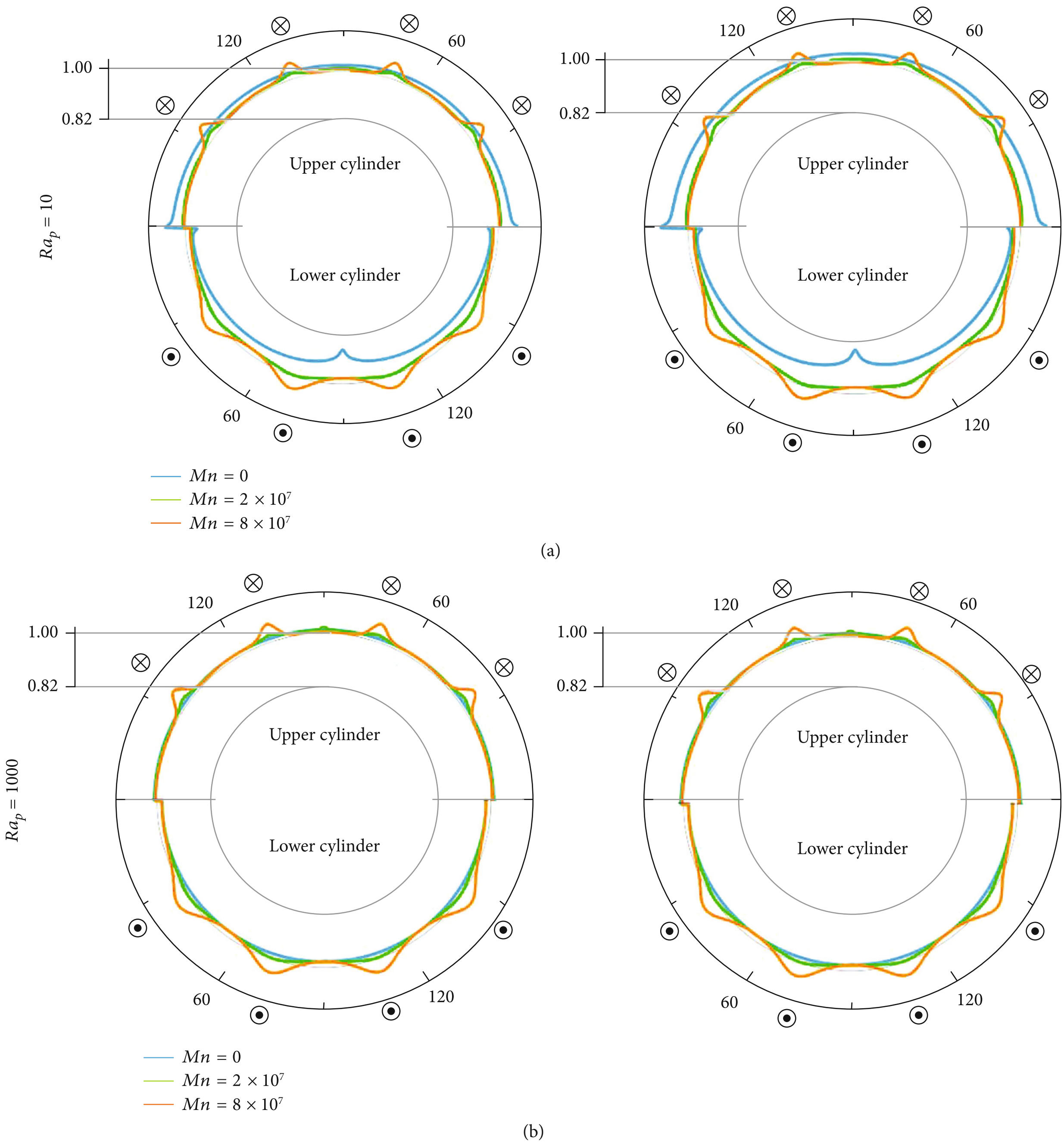

FIGURE 2: Nondimensional distribution of nanoparticles on the outer and inner cylinder walls for $\varphi_{\mathrm{Ave}} = 0.03$, $Ra_p = 10$ and 1000, and different magnetic numbers at (a) $\varepsilon = 0.4$ and (b) $\varepsilon = 0.7$.

Total entropy generation and the total Bejan number are obtained by integrating the relations of local entropy generation and Bejan number.

$$S_{T,HT} = \int_A S_{L,HT} dA, S_{T,FF} = \int_A S_{L,FF} dA, S_{T,s} = \int_A S_{L,s} dA, Be_{\mathrm{ave}} = \frac{\int_A Be_L dA}{\int_A dA}. \tag{10}$$

4. CFD Setting

The presented nonlinear governing PDE equations are solved based on finite volume method (FVM). The continuity and momentum equations are coupled and solved in an algorithm termed SIMPLE. The energy and concentration equations simultaneously solved. The advection terms in the governing equations are discretized based on first-order upwind schemes, and diffusion terms are solved based on second-order central schemes. The numerical convergence criterion was residual values. The

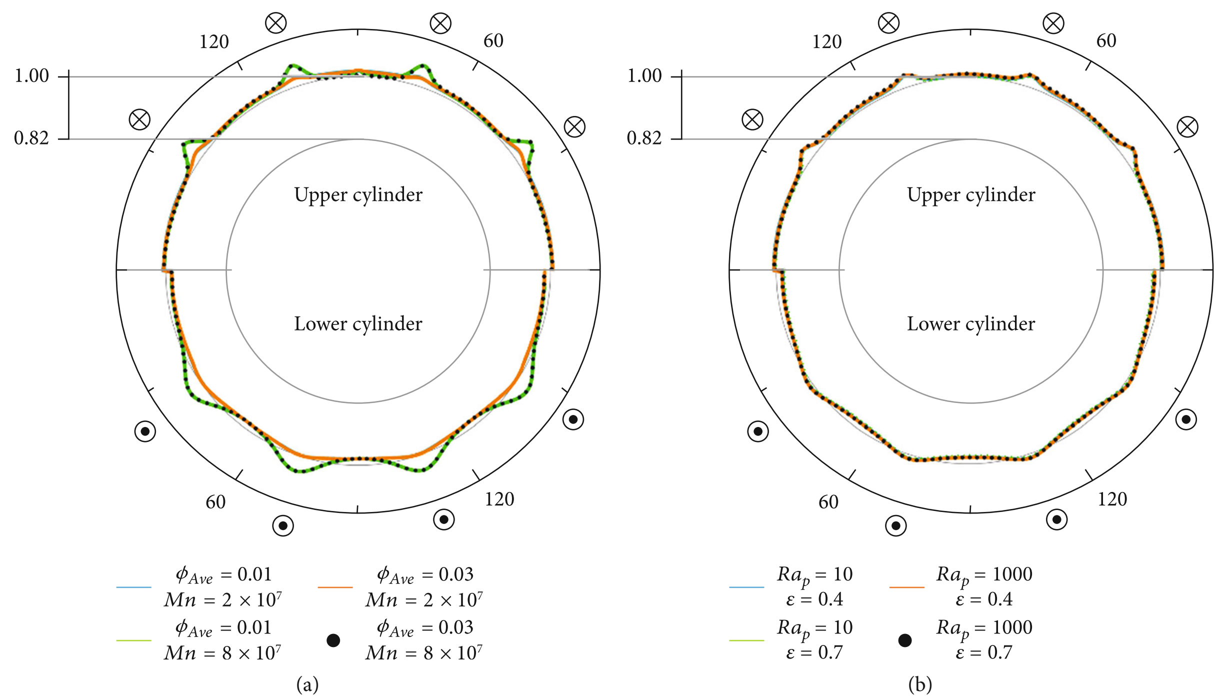

FIGURE 3: Nondimensional distribution of nanoparticles on inner and outer walls (with angle of ζ) for (a) different magnetic numbers and volume fraction at $Ra_p = 1000$ and $\varepsilon = 0.7$, (b) different porous Rayleigh number and porosity at $\varphi_{\mathrm{Ave}} = 0.03$ and $Mn = 8 \times 10^7$.

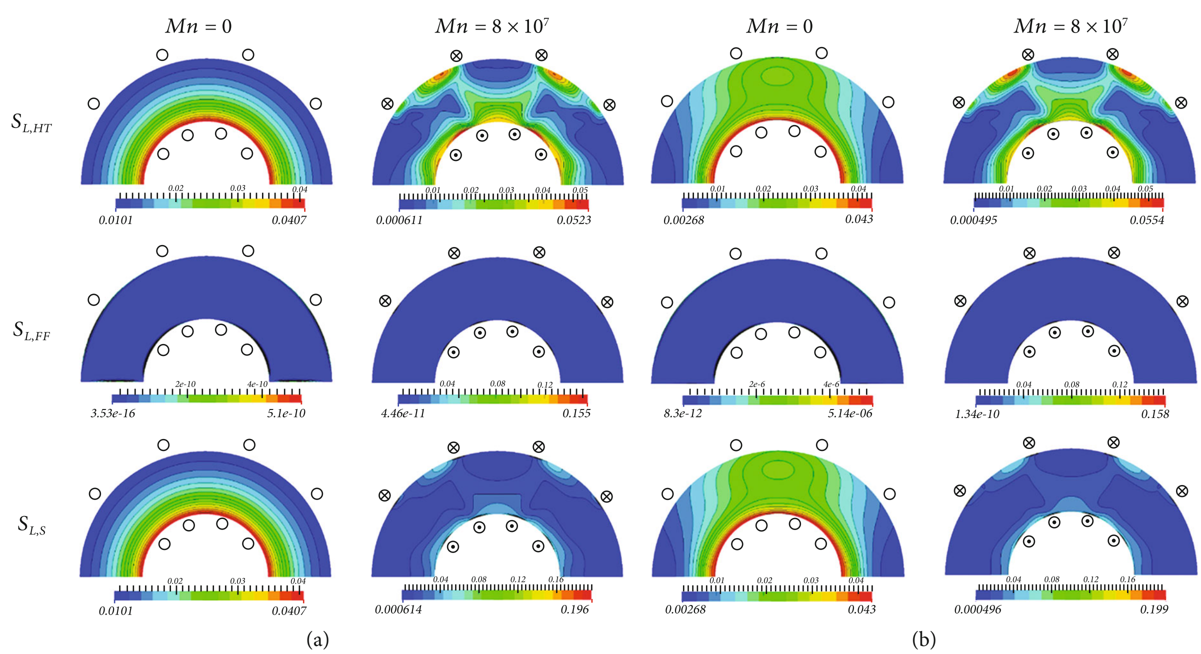

FIGURE 4: The dimensionless local entropy generation due to heat transfer ($S_{L,HT}$), fluid friction ($S_{L,FF}$) and summation ($S_{L,s}$) for $\varphi_{\mathrm{Ave}} = 0.03$, $\varepsilon = 0.7$, and $Mn = 0$ and 8×10^7 at (a) $Ra_p = 10$ and (b) $Ra_p = 1000$.

residual values at convergence for velocity and pressure fields were 10^{-5}, and for temperature and φ were 10^{-6}. Under relaxation factors for velocity, pressure, temperature, and φ were 0.4, 0.6, 0.2, and 0.01, respectively. Square uniform mesh is selected for presented study, based on nanoparticle distribution on the hot wall 40,000 (200×200) numbers of mesh selected. Moreover, for validation of the entropy generation, the results of the present study is compared with the work of Shavik et al. [33] (Table 1). In all cases, the results of this study are in good agreement.

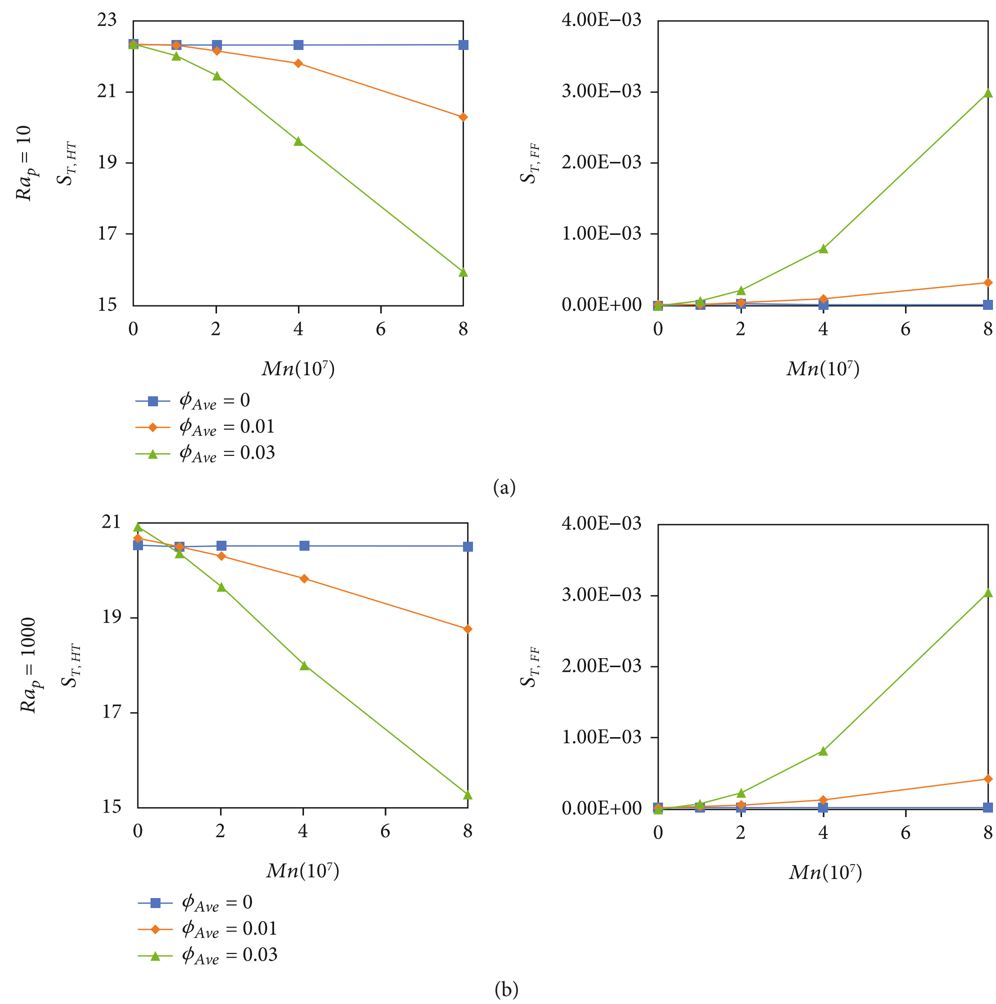

FIGURE 5: Dimensionless total entropy generation due to heat transfer ($S_{T,HT}$) and fluid friction ($S_{T,FF}$) for $\varepsilon = 0.7$ and different volume fraction of nanoparticle.

5. Results and Discussion

Extended Buongiorno's two-phase model is considered for the distribution of nanoparticles. The numerical simulation has investigated for porous Rayleigh number ($Ra_p = 10$ and 1000), the volume fraction of nanoparticles ($\varphi_{\mathrm{Ave}} = 0, 0.01$ and 0.03), porosity number ($\varepsilon = 0.4$ and 0.7), and magnetic number ($0 \leq Mn \leq 8 \times 10^7$). Constant values included $\mathrm{Pr} = 4.623$, $Sc = 3.55 \times 10^4$, $T_c = 310\,K$, $q'' = 48.01\,(w/m^2)$, $1.71 \times 10^5 < Le < 6.84 \times 10^5$, $Da = 10^{-3}(K = 0.625 \times 10^{-6})$, $\delta = 161$, $N_{BT} = 0.245$, $X = 3 \times 10^{-11}$, and $T_m = T_c + Lq''/2k_f = 310.96\,K$.

The effects of the mentioned parameters have studied the distribution of nanoparticles and the entropy generation contours due to fluid friction and heat transfer, and Bejan.

Figure 2 shows the nondimensional distribution of nanoparticles on the lower and upper cylinder walls in $\varphi_{\mathrm{Ave}} = 0.03$ and $Ra_p = 10$ and 1000 for the different magnetic numbers. In Figure 2(a) and porous Rayleigh number 10, the density of nanoparticles is higher on the top wall (cold) than the down wall (hot); that is due to the thermophoresis term in the volume fractional equation. With the rising of porous Rayleigh number, the dimensional distribution of nanoparticles is almost identical due to the increasing flow velocity on the inner and outer walls. By increasing the magnetic number to $Mn = 2 \times 10^7$ for all of the cases, the density of nanoparticles for both walls is almost equal to the unit value, and no change occurs. But with the increasing magnetic number to $Mn = 8 \times 10^7$, the peak of nanoparticle density appears near the wires, which is due to the absorption of nanoparticles by the magnetic field. The above arguments are also true for Figure 2(b), which the porosity has increased to 0.7. Besides, in all graphs, the peak of nanoparticle density in the inner wall is wider than the outer wall.

Figure 3 shows a better comparison of the effect of different parameters on the dimensional distribution of nanoparticles. Figure 3(a) is shown for magnetic numbers and different volume fractions in $Ra_p = 1000$ and $\varepsilon = 0.7$. The dimensionless nanoparticle density is the same for the volume fraction 0.01 and 0.03 in a constant magnetic number. Therefore, the volume fraction does not affect the dimensionless distribution of nanoparticles. Also, in a constant volume fraction, the density of nanoparticles increases near

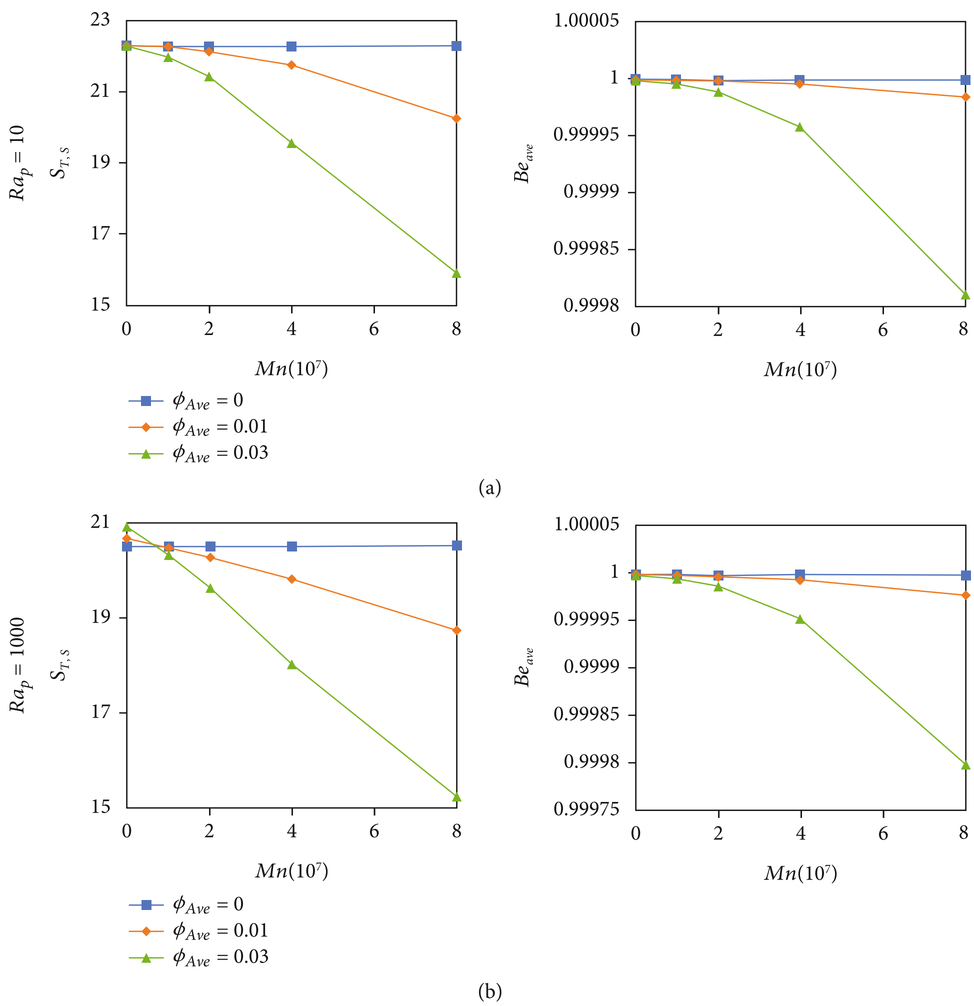

FIGURE 6: Dimensionless total entropy generation due to summation ($S_{T,s}$) and Bijan number for $\varepsilon = 0.7$ and different volume fraction of nanoparticle.

the wires due to increasing the magnetic number. Figure 3 (b) is plotted for different porosity and porous Rayleigh number in $\varphi_{\text{Ave}} = 0.03$ and $Mn = 8 \times 10^7$. Porosity and porous Rayleigh numbers do not affect on the dimensionless distribution of nanoparticles at the high magnetic field.

Figure 4 illustrates the dimensionless local entropy generation due to heat transfer ($S_{L,HT}$) and fluid friction ($S_{L,FF}$) and summation ($S_{L,s}$) inside a semiannulus for $\varphi_{\text{Ave}} = 0.03$, $\varepsilon = 0.7$, and $Mn = 0$ and 8×10^7 for different porous Rayleigh number. In Figure 4(a) in the absence of a magnetic field and $Ra_p = 10$, the $S_{L,HT}$ contours are similar to temperature contours. The highest value of $S_{L,HT}$ is on the inner cylinder wall (hot) due to extreme temperature gradients. In Figure 4(b), as increasing porous Rayleigh number to 1000, the shape of the contours $S_{L,HT}$ changes completely, in such a way that the densities of the contours increase near the inner cylinder wall and a core is created near the outer cylinder wall. By adding a magnetic field, the density of $S_{L,HT}$ contours increase near the wires, and, with the rise of porous Rayleigh number, there is no change in the shape of the contours. In all cases, due to gradients of high velocity on the walls and near the wires, the maximum value of $S_{L,FF}$ are in these regions. By comparing the values of $S_{L,HT}$ and $S_{L,FF}$, it can be seen that the effects of entropy generation due to heat transfer are much greater than the entropy generation due to fluid friction. As a result, the contours $S_{L,s}$ are very similar to $S_{L,HT}$ contours.

Figure 5 presents total entropy generation due to the heat transfer ($S_{T,HT}$) and fluid friction ($S_{T,FF}$) for the $\varepsilon = 0.7$ and different volume fractions of nanoparticle in porous Rayleigh numbers 10 and 1000. According to Figure 5(a), by intensifying the magnetic field for both porous Rayleigh numbers, $S_{T,HT}$ decreases linearly for the volume fraction of nanoparticles 0.01 and 0.03. In Figure 5(b), by intensifying the magnetic field at both porous Rayleigh numbers 10 and 1000, $S_{T,FF}$ decreases linearly and nonlinearly for volume fractions 0.01 and 0.03, respectively. Also, in all cases and the absence of a magnetic field, the value of $S_{T,FF}$ is almost zero. Figure 6(a) shows the dimensionless summation total entropy generation ($S_{T,s}$) at $\varepsilon = 0.7$ and different volume fraction of nanoparticles. According to the charts, the charts of $S_{T,s}$ are similar to $S_{T,HT}$ charts, because of the values of $S_{T,HT}$ dominates the values of $S_{T,FF}$. Also, according to Figure 6(b), with the increasing magnetic number for both porous Rayleigh numbers, Bejan number decreases linearly and nonlinearly for volume fractions 0.01 and 0.03, respectively.

6. Conclusion

In present work, effects of porous Rayleigh number, the volume fraction of nanoparticles, porosity, and magnetic number are investigated on nondimensional distribution of nanoparticles and entropy generation. The main findings can be condensed following point:

(i) Adding a magnetic field increases the distribution of nanoparticles near the wires and causes the formation of vortices and increasing the flow velocity

(ii) In the presence of the nonuniform magnetic field, with the increasing porosity and porous Rayleigh number, the distribution of nanoparticles becomes uniform. But, in the absence of a magnetic field, porosity and porous Rayleigh number do not affect the dimensionless distribution of nanoparticles

(iii) By increasing magnetic number and volume fraction of nanoparticles, Bejan number, entropy generation due to heat transfer, and summation decrease but entropy generation due to fluid friction increases

(iv) Entropy generation due to heat transfer is much greater than the entropy generation due to fluid friction

(v) With increasing the magnetic number, entropy generation due to fluid friction increases near the wires

Data Availability

No data were used to support this study.

Conflicts of Interest

There is no conflict of interest regarding the publication of this article.

Acknowledgments

The authors extend their appreciation to the Deanship of Scientific Research at King Khalid University for funding this work through research groups under grant number R.G.P.1/157/42. Also, this paper is supported by Shaanxi Key Research and Development Plan (Grant No. S2021-YF-YBGY-0708) and the authors extend their sincere appreciation to Princess Nourah bint Abdulrahman University Researchers Supporting Project number (PNURSP2022R46), Princess Nourah bint Abdulrahman University, Riyadh, Saudi Arabia.

References

[1] X. Zhang, Y. Tang, F. Zhang, and C. S. Lee, "A novel aluminum–graphite dual-ion battery," *Advanced Energy Materials*, vol. 6, no. 11, p. 1502588, 2016.

[2] M. Wang, C. Jiang, S. Zhang, X. Song, Y. Tang, and H. M. Cheng, "Reversible calcium alloying enables a practical room-temperature rechargeable calcium-ion battery with a high discharge voltage," *Nature Chemistry*, vol. 10, no. 6, pp. 667–672, 2018.

[3] S. Mu, Q. Liu, P. Kidkhunthod, X. Zhou, W. Wang, and Y. Tang, "Molecular grafting towards high-fraction active nanodots implanted in N-doped carbon for sodium dual-ion batteries," *National Science Review*, vol. 8, no. 7, p. nwaa178, 2021.

[4] X. Liu, G. Zhang, J. Li et al., "Deep learning for Feynman's path integral in strong-field time-dependent dynamics," *Physical Review Letters*, vol. 124, no. 11, article 113202, 2020.

[5] W. Yang, Y. Lin, X. Chen et al., "Wave mixing and high-harmonic generation enhancement by a two-color field driven dielectric metasurface [invited]," *Chinese Optics Letters*, vol. 19, no. 12, article 123202, 2021.

[6] S. Y. Motlagh, E. Golab, and A. N. Sadr, "Two-phase modeling of the free convection of nanofluid inside the inclined porous semi-annulus enclosure," *International Journal of Mechanical Sciences*, vol. 164, article 105183, 2019.

[7] E. Golab, S. Goudarzi, H. Kazemi-Varnamkhasti et al., "Investigation of the effect of adding nano-encapsulated phase change material to water in natural convection inside a rectangular cavity," *Journal of Energy Storage*, vol. 40, article 102699, 2021.

[8] A. N. Sadr, M. Shekaramiz, M. Zarinfar, A. Esmaily, H. Khoshtarash, and D. Toghraie, "Simulation of mixed-convection of water and nano-encapsulated phase change material inside a square cavity with a rotating hot cylinder," *Journal of Energy Storage*, vol. 47, article 103606, 2021.

[9] B. Vahedi, E. Golab, A. N. Sadr, and K. Vafai, "Thermal, thermodynamic and exergoeconomic investigation of a parabolic trough collector utilizing nanofluids," *Applied Thermal Engineering*, vol. 206, article 118117, 2022.

[10] Y. Cao, M. A. Abdous, S. G. Holagh, M. Shafiee, and M. Hashemian, "Entropy generation and sensitivity analysis of R134a flow condensation inside a helically coiled tube-in-tube heat exchanger," *International Journal of Refrigeration*, vol. 130, pp. 104–116, 2021.

[11] C. Liu, M. Hashemian, A. Shawabkeh et al., "CFD-based irreversibility analysis of avant-garde semi-O/O-shape grooving fashions of solar pond heat trade-off unit," *Renewable Energy*, vol. 171, pp. 328–343, 2021.

[12] Y. Cao, H. Ayed, S. Jafarmadar et al., "PEM fuel cell cathode-side flow field design optimization based on multi-criteria analysis of liquid-slug dynamics," *Journal of Industrial and Engineering Chemistry*, vol. 98, pp. 397–412, 2021.

[13] M. Abbasi, A. N. Esfahani, E. Golab et al., "Effects of Brownian motions and thermophoresis diffusions on the hematocrit and LDL concentration/diameter of pulsatile non-Newtonian blood in abdominal aortic aneurysm," *Journal of Non-Newtonian Fluid Mechanics*, vol. 294, article 104576, 2021.

[14] Y. Cao, H. Ayed, H. S. Dizaji, M. Hashemian, and M. Waehayee, "Entropic analysis of a double helical tube heat exchanger including circular depressions on both inner and outer tube," *Case Studies in Thermal Engineering*, vol. 26, article 101053, 2021.

[15] S. Goudarzi, M. Shekaramiz, A. Omidvar, E. Golab, A. Karimipour, and A. Karimipour, "Nanoparticles migration due to thermophoresis and Brownian motion and its impact on Ag-MgO/water hybrid nanofluid natural convection," *Powder Technology*, vol. 375, pp. 493–503, 2020.

[16] M. Aliakbari, "Numerical investigation of heat transfer of nanofluids in a channel under the influence of porous area," *Journal of Fundamental and Applied Sciences*, vol. 9, pp. 1175–1188, 2017.

[17] M. Ahmadi, F. Dashti Ahangar, N. Astaraki, M. Abbasi, and B. Babaei, "FWNNet: presentation of a new classifier of brain tumor diagnosis based on fuzzy logic and the wavelet-based neural network using machine-learning methods," *Computational Intelligence and Neuroscience*, vol. 2021, Article ID 8542637, 13 pages, 2021.

[18] Y. Cao, H. Ayed, M. Hashemian, A. Issakhov, and M. Waehayee, "Thermal/frictional performance of spiral pipe with ring-shape depression used as in-pond heat exchanger," *Solar Energy*, vol. 224, pp. 742–756, 2021.

[19] M. Siavashi, H. R. Talesh Bahrami, and H. Saffari, "Numerical investigation of flow characteristics, heat transfer and entropy generation of nanofluid flow inside an annular pipe partially or completely filled with porous media using two-phase mixture model," *Energy*, vol. 93, pp. 2451–2466, 2015.

[20] M. V. Bozorg, M. Hossein Doranehgard, K. Hong, and Q. Xiong, "CFD study of heat transfer and fluid flow in a parabolic trough solar receiver with internal annular porous structure and synthetic oil- Al_2O_3 nanofluid," *Renewable Energy*, vol. 145, pp. 2598–2614, 2020.

[21] M. T. Jamal-Abad, S. Saedodin, and M. Aminy, "Experimental investigation on a solar parabolic trough collector for absorber tube filled with porous media," *Renewable Energy*, vol. 107, pp. 156–163, 2017.

[22] M. Corcione, M. Cianfrini, and A. Quintino, "Two-phase mixture modeling of natural convection of nanofluids with temperature-dependent properties," *International Journal of Thermal Sciences*, vol. 71, pp. 182–195, 2013.

[23] Y. A. Al-Turki, H. Moria, A. Shawabkeh, S. Pourhedayat, M. Hashemian, and H. S. Dizaji, "Thermal, frictional and exergetic analysis of non-parallel configurations for plate heat exchangers," *Chemical Engineering and Processing-Process Intensification*, vol. 161, article 108319, 2021.

[24] S. Göktepe, K. Atalik, and H. Ertürk, "Comparison of single and two-phase models for nanofluid convection at the entrance of a uniformly heated tube," *International Journal of Thermal Sciences*, vol. 80, no. 1, pp. 83–92, 2014.

[25] J. Buongiorno, "Convective transport in nanofluids," *Journal of Heat Transfer*, vol. 128, no. 3, pp. 240–250, 2006.

[26] N. Anbuchezhian, K. Srinivasan, K. Chandrasekaran, and R. Kandasamy, "Thermophoresis and Brownian motion effects on boundary layer flow of nanofluid in presence of thermal stratification due to solar energy," *Applied Mathematics and Mechanics*, vol. 33, no. 6, pp. 765–780, 2012.

[27] E. Kaloudis, E. Papanicolaou, and V. Belessiotis, "Numerical simulations of a parabolic trough solar collector with nanofluid using a two-phase model," *Renewable Energy*, vol. 97, pp. 218–229, 2016.

[28] S. A. Farshad and M. Sheikholeslami, "Nanofluid flow inside a solar collector utilizing twisted tape considering exergy and entropy analysis," *Renewable Energy*, vol. 141, pp. 246–258, 2019.

[29] C. Ò. Vp-, A. Mwesigye, Z. Huan, and J. P. Meyer, "Thermal performance and entropy generation analysis of a high concentration ratio parabolic trough solar collector with Cu-Therminol®VP-1 nanofluid," *Energy Conversion and Management*, vol. 120, pp. 449–465, 2016.

[30] S. K. Verma, A. K. Tiwari, and D. S. Chauhan, "Experimental evaluation of flat plate solar collector using nanofluids," *Energy Conversion and Management*, vol. 134, pp. 103–115, 2017.

[31] M. Sheikholeslami, A. Arabkoohsar, I. Khan, A. Shafee, and Z. Li, "Impact of Lorentz forces on Fe_3O_4-water ferrofluid entropy and exergy treatment within a permeable semi annulus," *Journal of Cleaner Production*, vol. 221, pp. 885–898, 2019.

[32] M. Afrand, A. Hajatzadeh, S. Aghakhani, and H. F. Oztop, "Free convection and entropy generation of a nanofluid in a tilted triangular cavity exposed to a magnetic field with sinusoidal wall temperature distribution considering radiation effects," *International Communications in Heat and Mass Transfer*, vol. 112, article 104507, 2020.

[33] S. M. Shavik, M. N. Hassan, A. M. Morshed, and M. Q. Islam, "Natural convection and entropy generation in a square inclined cavity with differentially heated vertical walls," *Procedia Engineering*, vol. 90, pp. 557–562, 2014.